Performance of a Ka-Band Transponder Breadboard for Deep Space Applications

N. R. Mysoor, S. Kayalar, J. P. Lane, and A. W. Kermode

Jet F'repulsion Laboratory
California Institute of T ethnology
Pasadena, California

Abstract. *This article summarizes the design concepts and implementation of an advanced Ka-band (34.4 GHz/32GHz) transponder breadboard for the next generation of space communications systems applications. 1 h e selected architecture upgrades the X-band (7.2GHz/8.4GHz) deep space transponder (DST) to provide Ka-band up/Ka- and X-band down capability. In addition, it can also be configured to provide X-band up/Ka- and X-band down. The Ka-band transponder breadboard incorporates several state-of-the-art components including sampling mixers, Ka-band dielectric resonator oscillator, and micro wave monolithic integrated circuits (MMICs). The MMICs that were tested in the breadboard include upconverters, down converters, automatic gain con trol circuits, mixers, phase modulators, and amplifiers. 7 he measured receiver dynamic range, tracking range, acquisition rate, static phase error, and phase jitter characteristics of the Ka-band breadboard interfaced to the advanced engineering model X-band DS1 are in good agreement with the expected performance. The results show a receiver tracking threshold of - 149dBm with a dynamic range of 80dB, and a down link phase jitter of 7° rms. 7he analytical results of phase noise and Allan standard deviation are in good agreement with the experimental results.*

Narayan R. Mysoor
email: narayan.mysoor@jpl.nasa.gov
tel: 818-354 -5s08

Sclahattin Kayalar
email: sclahattin.kayalar@jpl.nasa.gov
tel:818-354-2872

Arthur W. Kermode
email:arthur.kermode@jpl.nasa.gov
tel: 818-354-5422

address: Jet Propulsion Lab. MS-161-213, 4800 Oak Grove Dr. Pasadena, CA 91109

John P. Lane
mail: j.lane@viasat.com
tel: 619-929-7524
address: VSAT 2290 Cosmos Court, Carlsbad, CA 92009

Performance of a Ka-Band Transponder Breadboard for Deep Space Applications

N. R. Mysoor, S. Kayalar, J.P.Lane, and A. W. Kermode

Jet Propulsion Laboratory
California Institute of 1 ethnology
Pasadena, California

Abstract. This article summarizes the design concepts and implementation of an advanced Ka bend (34.4 GHz/32GHz) transponder breadboard for the next generation Of space communications systems applications. The selected architecture upgrades the X-band (7.2 GHz/8.4GHz) deep space transponder (DST) to provide Ka-band up/Ka- and X-band down capability. In addition, it can also be configured to provide X-band up/Ka- and X-bend down. The Ka -band transponder breadboard incorporates several state of-the-art components including sampling mixers, Ka-band dielectric resonator oscillator, and microwave monolithic integrated circuits (MMICs). The MMICs that were tested in the breadboard include upcon verters, downconverters, automatic gain control circuits, mixers, phase modulators, and amplifiers. The measured receiver dynamic range, tracking range, acquisition ra te, sta tic phase error, and phase jitter characteristics of the Ka band breadboard interfaced to the advanced engineering model X-band 0S7 are in good agreement with the expected performance. The results show a receiver tracking threshold of - 149dBm with a dynamic range of 80dB, and a downlink phase jitter of 7° rms. The analytical results of phase noise and Allan standard deviation are in good agreemen t with the experimental results.

L Introduction

Telecommunication transponders for deep space spacecraft applications [1,2] provide uplink command, turnaround ranging, differential one-way ranging, downlink telemetry, and radiometric capabilities. The Ka-band transponder breadboard provides these capabilities at Ka-band uplink [3] frequency of 34.415GI Iz and downlink frequency of 31.977GI Iz. Operation at Ka-band allows the use of smaller antenna, and provides higher transmission bandwidth to allow 4dB to 6dB improvement over X-band on downlink data rate capability and provides increased accuracy in differential one-way ranging applications. Furthermore, Ka-band has a unique advantage for missions such as Solar Probe, Mercury, and Venus missions as it suffers negligible signal-to noise degradation due to signal scintillation in the solar plasma. The signal-to-noise degradation at X-band is estimated to be about 5 to 10dB in solar flux environment.

To enable flexibility in spacecraft design and modularity in spacecraft hardware, the design was chosen to provide the Ka-trand functionality by adding conversion circuitry to the existing X-band (7.2GI Iz/8.4GI Iz) deep space transponder (DST) design [2] as shown in Figure 1. This modularity allows either X- or Ka-band uplink and X- and/or Ka-band downlink operation.

This article describes the Ka-band transponder design, analysis, and breadboard performance results. The Ka-band transponder block diagram, functional requirements, and design specifications arc summarized in Section 11. The transponder phase noise analysis is described in Section 111. The breadboard performance rc.suits and conclusions arc presented in Sections IV and V, respectively.

II. Ka-Band Transponder Block Diagram and Requirements

The Ka band transponder functional block diagram and frequency generation scheme are shown in Figure 1. The Ka-band transponder design uses the X-band DST and Ka-band receiver and exciter circuitry to implement the transponder functions at Ka-band uplink and downlink frequencies [2.,3]. The Ka-band receiver and exciter circuits arc designed to interface directly with either the X-band DST breadboard or the X-band DST Advanced Engineering Model (DST-AEM) developed by MOTOROLA for JPL. The Ka-band receiver circuitry performs preselection and low noise amplification at Ka-band and downconversion to the X-band DST uplink frequency. The Ka-band exciter circuitry performs telemetry, ranging and differential one-way ranging (DOR) phase modulation on the X-band DST downlink reference and frequency multiplication and conversion to the Ka band downlink frequency.

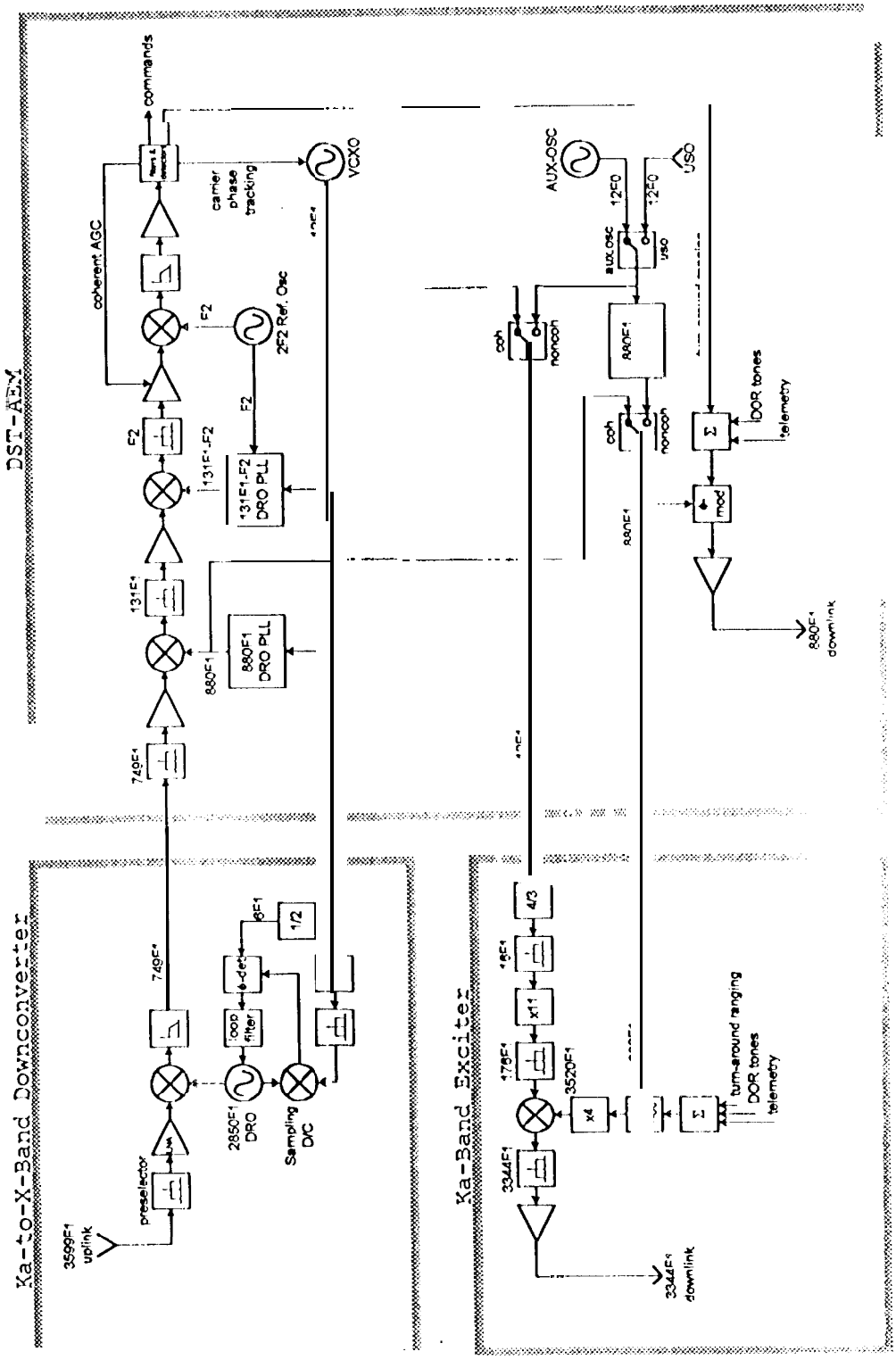

Figure 1. Ka-band transponder functional block diagram

Table 1. Ka-Band Transponder Design Requirements

Parameter	Design Requirements
1. Uplink frequency allocation:	
Ka-band uplink	34200 to 34700MHz, deep space
X-band uplink	7145 to 7190MHz, deepspace
2 Downlink frequency allocation:	
G-band downlink	31800 to 32300MHz, deep space
X-band downlink	8400 to 8450MHz, dee, space
3. Frequency translation ratios:	
Channel 14Ka-banduplink frequency	34415.4375 MHz ($3599F_1$)
Channel 14 X-trend uplinkfrequency	7162.312S MHz ($749F_1$)
X-band downlink	S80/3599 (8415 MHz)
Ka-band downlink	3344/3599 (31977MHz)
4. Ka-band Receiver Parameters:	
Carrier threshold	≤-149 dBm, unmodulated carrier
Dynamic range	≥ 79 dB (carrier threshold to -70 dBm)
Noise figure at Ka-band receiver input	≤ 6 dB
Acquisition and tracking rate	≥ 550 Hz/s at carrier Level > -110 dBm
Tracking range	≥ ±100 kHz minimum
Tracking error	≤ 1°/40 kHz at carrier level > -110 dBm
Capture range	≥ ±1 3 kHz at carrierlevel> -110 dBm
5. Ka-bandExciter Parameters:	
Frequency for coherent operation	3344/3599 times uplink frequency
Frequency for noncoherent operation	31987.32D988 MHz ($3344F_0$)|channel16
RF output power level	≥ + 3 dBm
output VSWR	≤ 1.5:1, 50 ± 5 ohms
Spurious signals	S -60 d Bc
Modulation bandwidth	≥ 50 MHz @ ± 0.5 dB
Peak phase modulation index	± 25 radians at ± 8-/0 linearity
Modulation sensitivity	? radians peak/vc,lt peak
Modulation index stability	± 10% over -20°C to +75°C
Modulation index:	
- Turnaround ranging	3-9 dB carrier suppression
- Telemetry	0-15 dB carrier suppression
- DOR	0 -1.1 dB carrier suppression
Residual phase noise (5 to 25Mt 17)	≤ 8° rms in the coherent mode
	S 8° rms in the noncoherent mode
Carrier phase delay variation	≤ 12 ns over -20°C to +75°C
Differential phase delay variation	≤ 2 m Ka-/X-band, over -20°C to +75°C
Ranging phase delay variation	≤ 30 ns Over-X3"C to + 75°C

The design requirements for the Ka-band transponder and frequency translation ratios arc. listed in 'l'able 1. The uplink and downlink frequencies are expressed in terms of the reference frequency F_1. The exact F_1 frequency is determined by the Deep Space Network (DSN) channel in operation. The DSN channel frequencies [2,3] selected for this implementation correspond to channel number 14 at $2F_1$ with F_1 equal to 9.5625MHz for coherent mode, and channel number 16 at $2F_0$ with F_0 equal to 9.565586MHz for noncoherent mode. The turnaround ratio of the uplink to downlink frequency is equal to 3599/3344 (34.4GHz/32GHz). The criteria [3] used in the selection of the turnaround ratio include maximum possible number of DSN channels for simultaneous X- and Ka-band operation, transmit/receive channel separation for diplexer implementation, central Ka- band allocation considerations, transponder implementation complexity, and uplink/downlink interference considerations

The design requirements shown in Table 1. apply to Ka-band receiver and exciter breadboards operating with the X-band DST-AEM. These requirements can be satisfied with no modifications to X-band DST-AEM. The Ka-band receiver performance include a noise figure of 5.4dB, an unmodulated carrier tracking threshold of -149dBm, and a tracking range of ±100kHz at the assigned channel frequency. The acquisition and tracking rate. is specified to be at least 550Hz/s. The specified nominal output power of the Ka-band exciter is +3dBm. The exciter output is phase modulated to a maximum phase deviation of ±2.5radians with a radio frequency ±0.5dB modulation bandwidth of 50MHz. The phase noise measured from 51 Iz to 25MHz is required to be less than 8° root mean square (rms) in the coherent mode, and 8° rms in the noncoherent mode.

A. X-band Deep Space **Transponder** Advancer! **Engineering** Model **Frequency** Plan. The functional block diagram for X-band Deep Space Transponder Advanced Engineering Model is shown in Figure 1. The X-band receiver [2] is implemented as a double-conversion superheterodyne phase-lock earner tracking receiver, with a fixed second intermediate frequency (IF). The first and second intermediate frequencies arc at $131F_1$ (1252.7MHz) and F_2 (12.25MHz), respectively. Coherent carrier automatic gain control (AGC) is employed in troth of the IF sections to provide a constant signal plus noise at the carrier loop phase detector. The first local oscillator (LO) signal at $880F_1$ (8415MI Iz) and the second LO signal at 1311(1-1;2 arc generated hy a dielectric resonator oscillator (DRO) [4] and a surface acoustic wave resonator oscillator (S1{0), respectively. Both of these oscillators arc phase locked to the $12F_1$ (1 14.75MHz) voltage controlled crystal oscillator (VCXO). The $12F_1$ VCXO is in turn phase locked to the uplink carrier. The SRO PLL consists of a SRO, a Xl 1 multiplier, a ÷6 divider, two mixers, a ÷2 divider, and a phase detector. The Xl 1 multiplier and ÷6 divider arc used in the SRO 1'1.1. to generate the frequencies $132F_1$ and $2F_1$ from $12F_1$. The $2F_1$ and the reference oscillator output at $2F_2$ arc applied to a mixer followed by a ÷2 divider to obtain a reference signal at F_1+F_2 to the SRO PLL phase detector. The SRO output at $131F_1-F_2$ and the $132F_1$ signals arc applied to a mixer to obtain the second input signal at F_1+F_2 to the SRO PLL phase detector. A x73 multiplier and a ÷3 divider arc used in the DRO 1'1.1. to generate reference signals at $836F_1$ and $4F_1$, respectively.

The coherent downlink carrier at $880F_1$ is provided by the LO DRO when the DST is operating in the coherent mode from the VCO. In the noncoherent mode, an $880F_0$ frequency is generated hy the exciter DRO phase locked to the DST $12F_0$ auxiliary oscillator (AUX OSC) or the external ultra stable oscillator (USO). The noncoherent downlink signal is automatically selected by the receiver AGC function upon the absence of an uplink signal. An X-band phase modulator is used to phase modulate the downlink signal with telemetry signals, turnaround ranging, or differential one-way ranging tones.

B. Ka-band to X-band Downconverter. The Ka-band receiver circuitry performs preselection and low noise amplification at $3599F_1$ (34.415CTI Iz) and downconversion to the $749F_1$ @.16GJ Iz) X-band DST uplink frequency. A 5 pole Chebychev waveguide iris preselector filter is used to filter the receiver Ka-band uplink frequency at 34.415G1 Iz, reject the Ka-band downlink frequency at 33441'1 (31 .977GHz), and attenuate the receiver LO leakage. After a waveguide-to-coax transition, a MMIC low noise amplifier (LNA) sets the noise figure of the receiver. A triple balanced hybrid mixer is used for downconversion to X-hand.

A phase locked Ka-band DRO generates the 1.0 signal at $2850F_1$ (27.253GHz) needed for the $3599F_1$ to $749F_1$ downconversion. The phase locked DRO yields lower spurious output (20 to 40dB) and phase noise than could be achieved with a direct multiplication implementation An hybrid MMIC sampling downconverter is used to sample the Ka-band LO output with a $36F_1$ reference and downconvert it to $6F_1$ for phase detection with a digital phase/frequency detector. The $6F_1$ and $36F_1$ loop references arc derived from the $12F_1$ reference with a divide-hy-two analog Miller divider and a BJT multiplier, respectively.

C. Ka-band Exciter. The Ka-band exciter circuitry performs phase modulation on the $880F_1$ (8.41 5GHz) X-hand DST downlink reference and frequency multiplication and conversion to the $3344F_1$ (31.977GHz) Ka-band downlink frequency. An X-band MMIC phase modulator [5] modulates the telemetry, ranging, and DOR signal on the X-Band DST downlink reference. The modulated X-Band signal is multiplied to $3520F_1$ (33.66GHz) with a hybrid x4 varactor multiplier The harmonics arc filtered to reduce inband spurious signals on the downlink The $3520F_1$ modulated signal is converted to the $3344F_1$ downlink frequency by mixing it with a $176F_1$ (1683MHz) signal using a MMIC upconverter. The conversion spurious signals arc filtered out. The $176F_1$ reference for the''conversion is, generated from the $12F_1$ reference signal from DST with a Miller divider and step-rccovcry diode multiplier. The Miller divider multiplies the $12F_1$ reference by 4/3 to give $16F_1$. The signal is multiplied with a x11 step recovery diode circuit and filtered to produce the $176F_1$ reference.

III. Ka-Band Transponder Phase Noise Analysis and Results

The downlink phase noise power spectral density of the Ka-band transponder is predicted using noise models [6- I 1] for various devices and the loop transfer fum tions in a custom JPL software package. The phase noise outputs of the local oscillator loops arc used in the receiver loop and the exciter to determine the resultant downlink phase noise. The loop transfer functions modify the noise spectral density of the individual contributors when referenced to the loop output. The models for phase noise contributors common to all loops arc developed first. These contributors include oscillators, varactors, phase detectors, buffer amplifiers, multipliers, dividers, operational amplifiers, power converter circuits, regulators, and phase modulators. These devices arc modelled with the appropriate white phase, flicker phase, white frequency, anti flicker frequency noise characteristics. The phase noise density of each contributor is modified by the transfer function from the contributor to the output. For example, the noise at the phase detector input will be modified by the receiver loop transfer function which is a low-pass response, whereas the noise at the 12F_1 VCO output will be modified by the loop error transfer function which is a high-pass response. The receiver phase noise at the phase locked VCO output is predicted by first calculating the contributions from the Ka-band, X-band, and L-band local oscillator circuits, and using these phase noise density functions in the receiver loop. The receiver VCO output phase noise density thus obtained is used in the exciter to predic t the coherent downlink phase noise density at Ka-band. The Ka-band downlink phase noise densities for the noncoherent AUX OSC mode is obtained by replacing the receiver VCO phase noise density by the AUX OSC oscillator phase noise density. The predicted theoretical phase noise results are compare.d to the measured results in the following section

IV. Experimental Results

The Ka hand transponder breadboard (Figure 1) consisting of the Ka-to-X-band downconverter, Ka-band exciter, and DST-AEM was implemented and performance characterization accomplished. The evaluation measurements include receiver tracking threshold sensitivity, static phase errors for Ka hand uplink frequency offset, swept acquisition characteristics, and AGC versus uplink signal level. All measurements were made at ambient room temperature. The measured tracking threshold sensitivity at the receiver best lock frequency, approximately channel center, is -149dBm. The measured receiver threshold characteristics show good correlation with expected performance (Appendix) over the tracking range as shown in Figure 2. The receiver acquisition characteristics were measured at an input signal level of -110dBm The measured values for tracking range, and tracking rate arc ±1.2MHz at design center frequency, and 800Hz/s, respectively, and meet the specified requirements (Table 1). No receiver false-lock or self-lock resulted during the test phase.

In the coherent carrier mode, residual phase noise is defined for a noise-free *received* signal case. The phase noise on the downlink carrier signal consists primarily of contributions from the four phased-locked oscillators 12F_1 VCO, SRO, X-band DRO, anti Ka-hand 1)RO used in the Ka-band transponder implementation. Individual phase noise power spectral density functions for these contributors arc used in a comprehensive computer program to predict the phase noise of the closed-loop receiver. Total residual phase noise in the output is the sum of the squares all noise sources. The predicted phase noise for the Ka-band transponder in the coherent mode is compared to the measured results in Figure 3. In the intervals between 5Hz and 25MHz on each side of the carrier, the root mean square phase noise is 7° rms, which is below the maximum allowable 8° for coherent downlink. The dominant contributor to this rms phase noise is the 12F_1 VCO and the x4 multiplication process from X-hand to Ka-band, the remaining contributions arc less than 10% of the VCO contribution Predicted nns phase noise and Allan deviation arc presented in Table 2. The results of the analysis indicate that the coherent mode specifications will be met for both the rms phase noise. The receiver PLL hand limits the VCO spectrum, thus providing the superior performance in the coherent mode.

A comparison of measured to calculated AlIan standard deviation characteristics as a function of integration time is shown in Figure 4. The measured AlIan standard deviation values for the Ka-band transponder breadboard arc in good agreement with the predicted values. Figure 5 shows good agreement between the theoretical and measured phase noise density curves for the noncoherent AUX OSC mode operation.

GaAs MMIC phase modulator [S] developed under SBIR contract at Pacific Monolithics Inc. was used to modulate the X-band reference signal and upconvert (x4 multiplication) it to Ka hand downlink signal as shown in Figure 1. The modulator MMIC chip incorporates a sin~lc-stage input buffer amplifier and a three-stage lumped element hybrid-coupled reflection phase shifters with MESFET varactors to provide a phase deviation of ±2.5radians with better than 8% linearity. The chip size is 2.49 X 0.91mm Sinusoidal and square

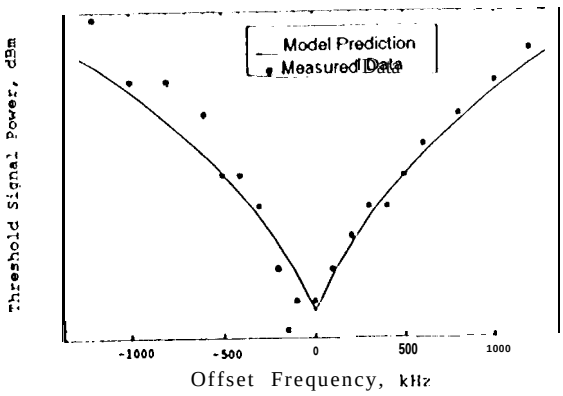

Figure 2. Ka-band transponder carrier tracking threshold vs offset frequency.

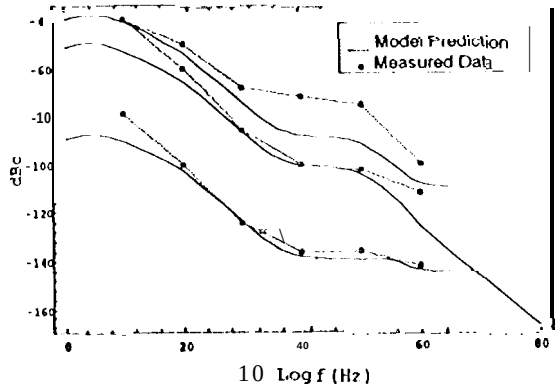

Figure 3. Comparison Of predicted and measured coherent-mode phase noise densities. (Uplink=-100dBm)

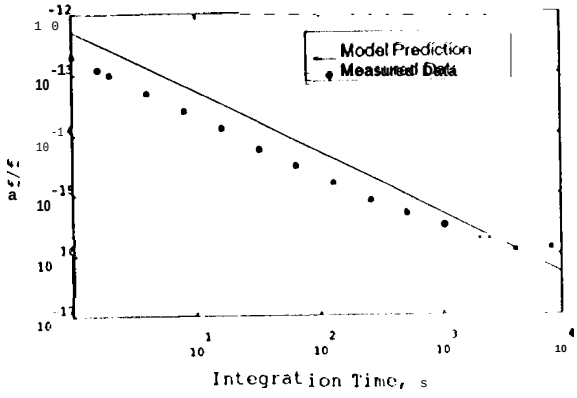

Figure 4. Ka-band transponder Allan deviation vs integration time.

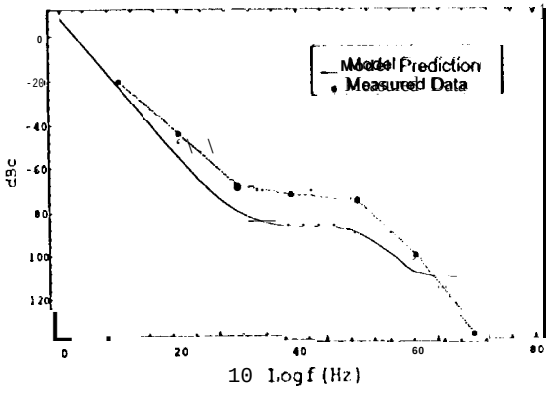

Figure 5. Comparison of the predicted and measured noncoherent-mode phase noise densities.

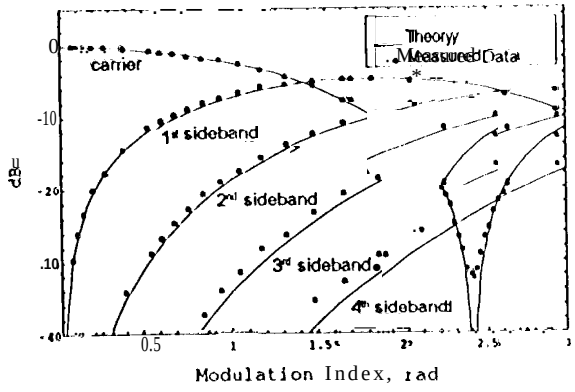

Figure 6. Measured and predicted Ka-band carrier, 1st, 2nd, 3rd, and 4th sideband levels vs. phase modulation index for the case of a sinusoidal modulating wave of 100-kHz frequency.

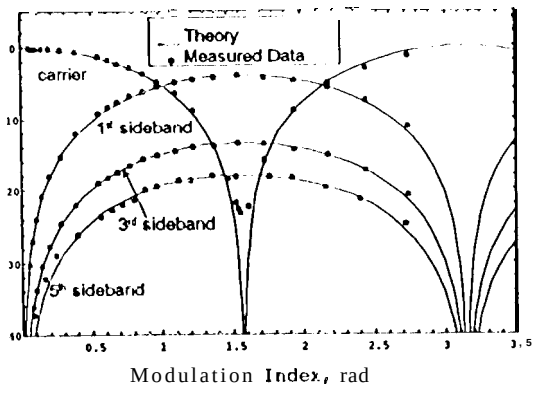

Figure 7. Measured and predicted Ka-band earner, 1st, 3rd, and 5th sideband levels vs. phase modulation index for the case of a square modulating wave of 100-kHz frequency.

Table 2 Predicted Phase Jitter and Allan Deviation for Coherent and Noncoherent Modes

Mode	Frequency	Phase Jitter (5Hz-25MHz) deg rms	Allan Deviation 0.01 sec	1 sec	1000 sec
COHERENT (Pc = -100dBm)	12F1	0.02	1.510-10	$1.3\ 10^{-12}$	$9.3\ 10^{-16}$
	880F1	0.80	$3.6\ 10^{-11}$	$4.6\ 10^{-13}$	$4.5\ 10^{-16}$
	3344F1	3.10	$4.6\ 10^{-11}$	$5.3\ 10^{-13}$	$4.9\ 10^{-16}$
NONCOHERENT AUX OSC	12F1	0.08	$6.1\ 10^{-10}$	$3.2\ 10^{-11}$	$3.2\ 10^{-11}$
	880F1	1.98	$4.8\ 10^{-11}$	$3.2\ 10^{-11}$	$3.2\ 10^{-11}$
	3344F1	7.60	$5.8\ 10^{-11}$	$3.2\ 10^{-11}$	$3.2\ 10^{-11}$

modulating waveforms were applied to the phase modulator and their resulting spectra [12,13] were monitored on a calibrated spectrum analyzer. All measurements were performed at ambient room temperature and with a carrier frequency of 31977MHz. A comparison of measured and predicted carrier, first, second and third sideband levels for the case of sinusoidal modulation is shown in Figure 6. A modulation frequency of 100kHz was used in the measurements.lhe peak phase modulation index range was adjusted from 0.2 to 2.4 radians. Figure 6 shows excellent agreement between theory and measurement for sinusoidal phase modulating waves. Negligible amplitude modulation distortion was observed in this case. A comparison of measured and predicted carrier, first, third and fifth sideband levels for the case of square-wave modulation is shown in Figure 7. A modulation frequency of 100kHz was used in the measurements. Good agreement between predicted and measured square-wave modulation results is demonstrated in Figure 7.

V. Conclusions

Design concepts and system architecture for a high performance Ka-band transponder for deep space spacecraft applications have been presented. The Ka-band transponder has been successfully breadhoarded and evaluated. New technologies such as a Ka-band DRO, X-hand MMIC phase modulator, MMIC amplifiers, MMIC upconverter, and sampling mixers have been integrated into the design. The Telecommunication Development 1 aboratory measurements on the breadboard transponder achieved a threshold level of -149dBm with a dynamic range of 80dB, and excellent acquisition and tracking characteristics. The measured phase noise, Allan standard deviation, and phase jitter data are in good agreement with the predicted characteristics. Measured carrier and relative sideband amplitudes resulting from phase modulation of the Ka-band downlink signal by sinusoidal and square-wave modulating functions agree well with the predicted results with negligible amplitude modulation distortion.

Acknowledgments

The research described in this paper was performed by the Jet I'repulsion Laboratory, California Institute of Technology, under contract with the National Aeronautics and Space Administration.

References

[1] J. H. Yuen, *Deep Space Telecommunications Systems Engineering*, Plenum Press, New York, 1983.

[2] N. R. Mysoor, J.D. Perret, and A W. Kermode, "Design Concepts and Performance of NASA X-Band (7162 Ml Iz/8415 MHz) Transponder for l)ecp-Space Spacecraft Applications," *TDA Progress Report* 42-104, *October-December* 1990, Jet I'repulsion Laboratory, Pasadena, California, February 1S, 1991, pp. 24'-?.56.

[3] J. A. Koukos, 'Selection of Ka-Band Transponder Turnaround Frequency Ratios," *Report of the Proceedings of RF and Modulation Subpanel 1E meeting at the German Spat-t Operations Center,* September 2(-24, 1993, CCSDS 11200-Y-1, consultative Committee for Space Data Systems, Oberpfaffenhofen, Germany, February 1994.

[4] N. R. Mysoor, "An Electronically Tuned, Stable 8415 MHz Dielectric Resonator FET Oscillator for Space Applications," Pmt. *IEEE* 1990 *Aerospace Applications Conference,* Vail, Colorado, February 5-9, 1990.

[5] N. R. Mysoor, and F. Ali, "Miniature X-Band GaAs MMIC Analog and Digital Modulators for Spaceborne Communications Applications," *Technology 2001 Conference Proceedings,* NASA Conference Publication 3136, vol. 1, San Jose, California, December 3-5, 1991, pp. 82-88.

[6] F. M. Gardner, *Phaselock Techniques,* John Wiley and Sons Inc., Ncw York, 1979.

[7] A. Blanchard, *Phase-Locked Loops: Applications to Coherent Receiver Design,* John Wiley and Sons Inc., New York, 1976.

[8] J. P. Frazier, and J. Page, "Phase-Lock Loop Frequency Acquisition Study," *IRE Trans. Set-8,* September 1962, pp. 210-227.

[9] D. B. Leeson, "A Simple Model of Feedback Oscillator Noise Spectrum," Pmt. *IEEE,* Vol. 54, February 1966, pp. 329-330.

[10] J. A. Barnes, A. R. Chi, and L. S. Cutler, *Characterization of Frequency Stability,* National Bureau of Standards Technical Note 394, Washington, D.C. National Bureau of Standards, October 197o.

[11] D. W. Allan, "Time and Frequency (Time Domain) Characterization, Estimation, and Prediction of Precision Clocks and oscillators," *IEEE Transactions on Ultrasonics, Ferroelectronics, and Frequency Control,* Vol. UFFC-34, No. 6, November 1987, pp. 647-654.

[12] N. R. Mysoor, and R. C). Mueller, "Performance of a 300-Degree Linear Analog Phase Modulator for Communications Applications," *Proc. of IEEE 1993 Aerospace Applications Conference,* Steamboat Springs, Colorado, February 1-5, 1993.

[13] E. A. Whitman, "Phase Modulation Measurement Techniques for Improved Accuracy," *Microwave Journal,* June 1978, pp. 113 116.

[14] F. Stocklin, *Relative Sideband Amplitudes vs. Modulation Index for Common Functions using Frequency and Phase Modulation,* Goddard Space Flight, Center. ,distributed by National Technical information Service, U. S. Department of Commerce, Springfield, Va, November 1973.

Appendix

The carrier tracking threshold of a 1'1.1. receiver [1 ,6,7] is defined as the minimum uplink signal required to maintain lock at any given offset from best lock frequency. It is a measure of an important limitation on spacecraft receiver performance.

At the best lock frequency, the carrier tracking threshold signal level is determined from the following equation:

$$\frac{SL}{kTF(2B_{LO})} = 1$$

where S is the receiver input signal power level, k is Boltzmann's constant, T is the reference system temperature, F is the receiver noise figure at the transponder input, B_{LO} is the one-sided noise-equivalrmt receiver carrier tracking loop bandwidth at threshold, and 1. is the receiver carrier channel loss. The calculated value of the worst case receiver carrier tracking threshold is equal to -149dBm for a $2B_{LO}$ of 721 Iz, channel loss of 1dB, and noise figure of 5.4dB (including isolator, filter, LNA, and connectors) at 290°K.

Note that the carrier tracking threshold signal level can also be expressed in terms of the variance of the phase error duc to additive channel noise hy

$$\sigma_\theta^2 = \frac{kTFB_{LO}}{SL} = \frac{1}{2}$$

Therefore at threshold the standard deviation of the phase error is $\sigma_\theta = 1/\sqrt{2}$. If the uplink signal frequency is offset from the best lock frequency by Δf Hz, the phase detector is required to operate with a static phase error of θ_e radians gives as

$$\theta_e = \sin^{-1}\left(\frac{2\pi\Delta f}{\alpha K_v}\right)$$

where K_v is the DC gain of the VCO., and α is the receiver limiter suppression factor given by

$$\alpha = 1\Big/\sqrt{1 + \frac{4}{n}\frac{kTFB_{if}}{SL}}$$

Here B_{if} is the noise equivalent predetection bandwidth. This static phase error reduces the threshold phase error standard deviation to $\sigma_\theta = 1/\sqrt{2} - \theta_e$, such that the carrier tracking threshold corresponding to the frequency offset of Δf Hz needs to satisfy

$$\sigma_\theta^2 = \frac{kTFB_{LO}}{SL} = \left(\frac{1}{\sqrt{2}} - \theta_e\right)^2$$

The one-sided noise equivalent carrier tracking loop bandwidth at threshold, B_{LO}, is given by

$$B_{LO} = \frac{1 + \left(K\tau_2^2/\tau_1\right)}{4\tau_2\left(1 + 1/\left(K\tau_2\right)\right)}$$

where τ_1 and τ_2 are the loop filter time constants, and K is the open loop gain of the PLL given by

$$K = \alpha K_v \cos(\theta_e) \exp\left(-\frac{1}{2}\left(\frac{1}{\sqrt{2}} - \theta_e\right)^2\right)$$

Note that the open loop gain of the PLL includes factors for the reduction of the phase detector sensitivity due to the static phase error and the additive channel noise.